The Fowler–Nordheim Plot Behavior and Mechanism of Field Electron Emission from ZnO Tetrapod Structures

Ahmed A. Al-Tabbakh,[†,*] Mahendra A. More,[‡] Dilip S. Joag,[‡] Imtiaz S. Mulla,[§] and Vijayamohanan K. Pillai[§]

[†]Department of Physics, Al-Nahrain University, Jadiriya 64055, Baghdad, Iraq, [‡]Center for Advanced Studies in Material Science and Condensed Matter Physics, Department of Physics, University of Pune, Pune 411007, India, and [§]Physical and Materials Chemistry Division, National Chemical Laboratory, Pune 411008, India

ABSTRACT Field emission measurements of current–voltage characteristics are reported for tetrapod structures of ZnO. The nonlinear Fowler–Nordheim (FN) plot is analyzed according to a model of calculation based on saturation of conduction band current and predominance of valence band current at high-field values. The simulated FN plot exhibits similar features to those observed experimentally. The model of calculation suggests that the slope variation of the FN plot, in the high-field and low-field regions, does not depend on the magnitude of saturation. Instead, it is a characteristic of the energy band structure and voltage-to-barrier-field conversion factor of the emitting material.

KEYWORDS: ZnO · field emission · Fowler–Nordheim plot · nonlinearity · nanostructures

Field emission properties of nanostructured ZnO have been investigated during the past decade by several researchers signifying compatibility and usefulness of this material as cold cathodes in flat panel displays and in vacuum microelectronic devices.[1−10] Despite being a wide band gap semiconductor, the analysis of the field emission properties and field emission mechanism has not been subjected to a particular model of calculations and has not been based on systematic comparison with the theoretical predictions. Results were explained through a general match/deviation of current–voltage ($I-V$) characteristics from the Fowler–Nordheim (FN) plot for metals. A careful investigation of the previous reports indicates that the experimental conditions and the dimensions of nanostructures affect the results profoundly.[1,3,4,7,8] In most of the earlier studies, the field emission characteristics were investigated in close proximity configuration, wherein the anode–cathode separation is less than 1 mm. Such a configuration poses a limitation on the strength of the applied electric field, as a relatively higher field value may lead to an arc formation. In such a configuration, the experimental FN plots are observed (fitted) to be linear. On the other hand, when experiments are performed in the conventional geometry of field emission microscopy, experimental FN plots exhibit a deviation from linearity, particularly in the high-field region.

For ZnO tetrapod-like structures deposited on a nickel substrate by the screen printing method, Wan *et al.* had investigated the field emission properties.[2] They described the FN plot behavior to be linear (metallic) despite that a clear deviation from linearity could be assigned. Recently, an experimental nonlinear characteristic of the FN plot has been reported for total current measurements of field emitted electrons from an isolated pod of ZnO tetrapod structure prepared by vapor deposition process.[8] The experimental results were analyzed as per the FN theory of metallic emitter.[11,12] For semiconducting emitters various effects such as the contribution of the effective electron mass and the work function dependence upon applied electrostatic field, limited generation rate of current carriers in p-type and lightly doped n-type semiconductors, and contribution of thermionic emission in low-field condition and surface states lead to nonlinear behavior of the FN plot. Rihon has done pioneering work on field emission mechanism and total energy distribution (TED) of field emitted electrons from a ZnO microtip.[13−16] Nevertheless, the experimental observations and the theoretical models have yet to offer a fitting explanation of the field emission mechanism in the context of a ZnO tetrapod structure. In this paper field emission probe–hole measurement of $I-V$ characteristics is presented for a single tetrapod structure of ZnO. Deviation from linear behavior is observed in the FN plot and

*Address correspondence to tabbakh2003@yahoo.com.

Received for review April 21, 2010 and accepted September 28, 2010.

Published online October 7, 2010.
10.1021/nn1008403

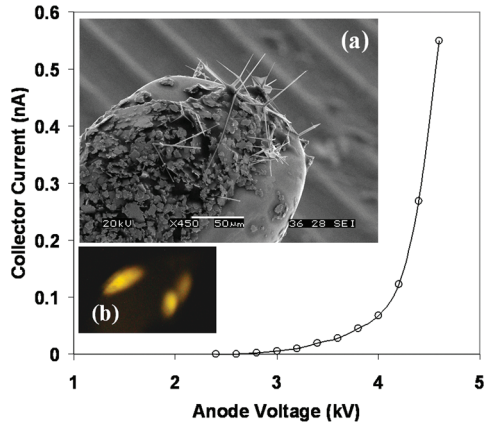

Figure 1. The probe−hole, *I*−*V* characteristics of a single pod of ZnO tetrapod structure at room temperature. Inset: (a) SEM image of ZnO tetrapod structures mounted on a tungsten microtip with the help of UHV compatible silver paste. (b) Field emission pattern; individual lobe is due to emission from a single pod.

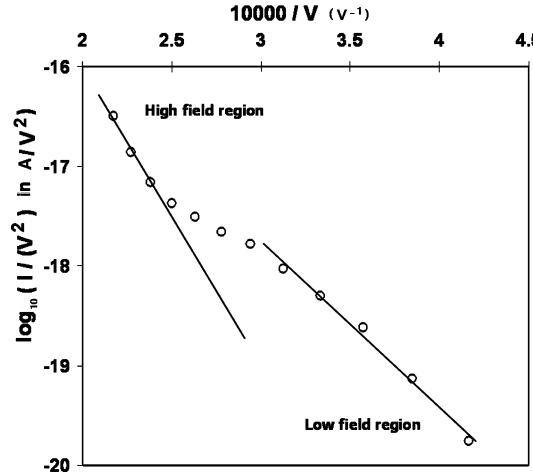

Figure 2. The probe−hole FN plot of field emitted electrons from a single pod of ZnO tetrapod structure. The figure shows clear deviation from linearity of FN plot at higher applied voltages, signifying the semiconducting nature of the ZnO.

is analyzed semiquantitatively using a model of calculation. It is shown that the nonlinear behavior is reproduced in the simulated FN plot due to the assumption of the conduction band current saturation at high-field values. Beside its consistence with the results, assumptions and conclusions obtained in the previous report of the TED measurements from the same batch of specimens, the present analysis is important for understanding of the field emission mechanism in ZnO nanostructures in particular and in structurally similar semiconducting emitters.[17] The simulated FN plot, produced from the calculation, exhibits similar features to those observed experimentally. The slope variation of the FN curve in the two regions of high and low fields is found to be independent of the saturation value. It is rather a characteristic of the energy gap and voltage-to-barrier-field conversion factor of the emitting material.

RESULTS AND DISCUSSION

The SEM image of the ZnO tetrapod structures mounted on the W tip is shown as an inset (a) in Figure 1. The image clearly reveals the presence of randomly oriented tetrapod structures on the W tip surface. The tetrapod structures possess lengths of few tens of micrometer with apex radii less than 200 nm (estimated from the magnified image which is not shown here for low quality). Before carrying out the measurements a high voltage was applied (4−5 kV), and the field emission pattern was observed on the anode screen (see inset (b) of Figure 1). The sample holder was then mechanically manipulated to bring a single lobe over the probe−hole of the analyzer. Optimization of the sample position has been discussed earlier.[17] Three different lobes, referring to emission from three individual pods of tetrapod structures, have been investigated. The probe−hole *I*−*V* plot of field emitted electrons from single pod of individual tetrapod structure is depicted in Figure 1. During the *I*−*V* measurement, the lens-to-anode voltage ratio ($V_L/V_A = 0.004$) was kept constant, the emitter was biased with −15 V with respect to the ground, and the collector current was measured for each anode voltage. The *I*−*V* characteristics exhibited an exponential-like behavior which was found to be reproducible for all investigated specimens.

Figure 2, the corresponding FN plot of the present *I*−*V* characteristics, shows a clear deviation from linearity at the high range of the applied voltages signifying the semiconducting nature of the ZnO emitter. The entire FN plot can be sectioned into three regions, two regions of linear behavior separated by a third (intermediate) region of lower slope as in the figure. This behavior of the FN plot was observed to be reproducible for all the ZnO tetrapod structures (belonging to the same synthesized batch). As stated earlier, Wan *et al.* also observed similar behavior of the FN plot for tetrapod-like structures despite the fact that they assigned the FN plot variation to be linear.[2] The slopes of the two linear sections, corresponding to low- and high-field regions were calculated from the least-squares fit to be −1.67 and −2.8, respectively. Assuming an average work function (H_{eff}) of the ZnO to be 5.3 eV, which is independent of the size and the aspect ratio of the tetrapod structure, the voltage-to-barrier-field conversion factor (β) from the following equation[18]

$$\text{slope}_{FN} = \frac{\partial \log_{10}(I/V^2)}{\partial(10^4/V)} = -2.9669 \times 10^3 \frac{H_{eff}^{3/2}}{\beta} s(y) \quad (1)$$

is calculated to be 2.1778×10^6 m^{-1}. This value is estimated by considering the slope of the linear section at low-field value which is claimed to be FN effective.[19] Assuming hemispherical geometry of the apex, the pod apex radius was estimated to be 91 nm. This value was calculated using $\beta = 1/(\alpha r)$ (where β is the observed value and $\alpha = 5$ for hemispherical geometry). Similarly,

the radius obtained from an iterative method was found to be 102 nm at $s(y) = 0.917$ and 3 kV applied voltage.[20] The estimated effective barrier height corresponding to the high-field region, using the same β factor (*of low-field region*), was found to be 7.64 eV. It indicates that the electrons originate from band(s) of about 2.34 eV below the conduction band minimum and contribute to the total emission current. The valence band maximum of the bulk ZnO lies 3.37 eV below the conduction band minimum subjected to the absence of the external electric field. The TEDs, measured for the same batch of specimen showed that emission from the valence band is possible due to intensification of the field at the pod apex of the tetrapod structure. Then, the underestimated value of the band gap energy (≈2.34 eV) may be attributed to various effects such as field penetration and band bending effects along with the lens effect of the probe−hole. It is true that the FN plot does not resolve the fine structure of the energy distribution of the field emitted electrons, but it describes rather well the emission current dependence on the applied field and the work function of the emitter. Following therefore, is an attempt to explain the field emission mechanism on the basis of the TEDs and the corresponding FN plots of the field emitted electrons.

NONLINEAR CHARACTERISTIC OF FN PLOT

A model calculation of the total emission current is obtained based on fundamental electron tunneling through a deformed surface potential barrier from typical band structure of bulk ZnO. TEDs of field emitted electrons suggest that the electrons originate from both the conduction band (CB) as well as the valence band (VB) with an energy separation equivalent to the band gap (E_g) of the bulk ZnO.[17] It is assumed that the distributions of the charge carriers in the two regions satisfy Fermi−Dirac (FD) statistics; therefore for the CB, emission usually comes from the degenerate energy band.[14] Similarly, for the VB, FD statistics is justified by the higher density of states than that of the CB.[21] In an approximation, the field emission from the *CB* and the *VB* is described by the standard FN equation with proper choice of the effective barrier height (H_{eff}) in the two regions $H_{eff} = H_{CB}$ and $H_{eff} = H_{VB} = H_{CB} + E_g$, respectively. Here, H_{CB} and H_{VB} refer to the energies of the conduction band minimum (CBM) and valence band maximum (VBM) measured with respect to the vacuum level, and E_g is the band gap energy. Therefore, the emission current from the two regions is treated according to the FN model, and emitted electrons are automatically replenished by other electrons from the interior of the substrate. The contribution of the surface states will be discussed in the end of this report. The total emission current I_{total} is the algebraic sum of the CB and VB currents (*i.e.*, I_{CB} and I_{VB}, respectively):[22]

$$I_{total} = I_{CB} + I_{VB} \quad (2)$$

where I_{CB} and I_{VB} are given by the FN equation:

$$I_{CB,VB} = \frac{aF^2A}{H_{eff}t^2(y)} \exp\left[\frac{-\upsilon(y)bH_{eff}^{3/2}}{F}\right] \quad (3)$$

$a = e^3/(8\pi h) = 1.54 \times 10^{-6}$ (A eV V^{-2}), $b = 4(2m)^{1/2}/(3\hbar e) = 6.83$ (eV$^{-3/2}$ V nm^{-1}), and A is the emitting area. F is the electric field strength given as $F = \beta V$ (where V is the applied voltage in volt and β is the voltage-to-barrier-field conversion factor in m^{-1}); $t(y)$ is a slowly varying function and $\upsilon(y)$ is a correction function due to image force approximation (Schottky−Nordheim barrier function).

Figure 3 shows the simulated $I-V$ characteristic of field emitted electrons from the CB and VB obtained by substituting β as 2.1778×10^6 m^{-1}(experimentally estimated). The functions $t(y)$ and $\upsilon(y)$ were determined algebraically from the standard formulas. The emitting area (A) was estimated as $A = 2\pi r^2$ where r is the radius of the single ZnO pod apex (91 nm). The corresponding FN plot of the total emission current is shown in the inset of Figure 3 which exhibits a linear characteristic. It is clear that the CB current predominates allover the range of the applied voltages which is obviously due to higher probability of barrier penetration at CB level (*i.e.,* VB electrons tunnel from energy level 3.37 eV below CB minimum). However, the FN plot shows no deviation from linearity, even at high values of applied fields. This is due to the exponential characteristic dependence of the current on the applied electric field, which is a result of the internal distribution function of the electrons (FD) assumed for both CB and VB. Numerical determination of the total emission current shows that CB current is at least 1 order of magnitude higher than the VB current at high applied voltages.

To shed more light on the experimentally observed nonlinear characteristic of the FN plot, it is attempted to consider the work of Baskin *et al.* regarding electron

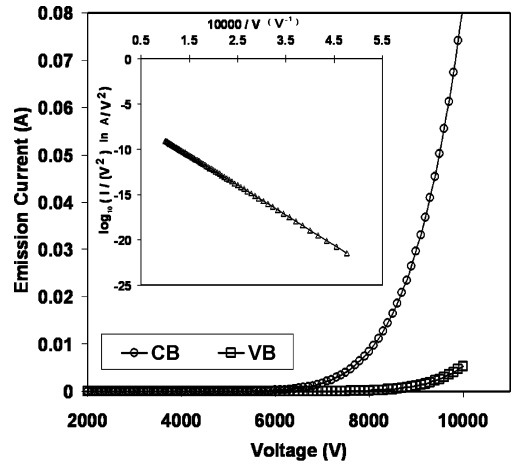

Figure 3. $I-V$ characteristics of field emitted electrons from conduction and valence bands. Inset: FN plot of the total emission current.

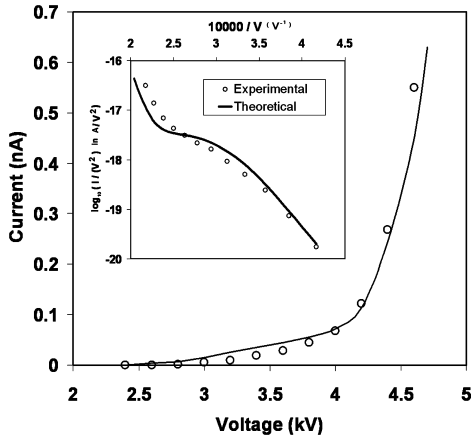

Figure 4. The fitting of the experimental probe−hole *I*−*V* characteristics and corresponding FN plot considering the assumption of (Baskin *et al.*) of the CB current saturation.

emission from the CB.[14] Baskin *et al.* have theoretically analyzed the field emission behavior of an n-type semiconductor based on field emission from CB only. The authors have concluded that the CB current acquires saturation at high-field values, which has been attributed to a limited generation rate of the current carriers inside the semiconductor. On the basis of the above conclusion and thereby imposing a saturation value of the CB current, we have obtained the *I*−*V* characteristics (Figure 4) as per eqs 2 and 3 using the same set of parameters defined in the previous paragraph. The condition of the CB current saturation implies the VB current to be predominant at all field values higher than that at which the CB current acquires saturation. Interestingly, the FN plot does not remain linear and shows an onset of deviation exactly at a point corresponding to saturation of the CB current (see inset of Figure 4, solid curve). The slope of the FN plot reduces over a short-range of field values until the VB current approaches the CB current saturation value and then increases as the VB current becomes considerably higher than the CB current. This behavior resembles that of the experimental FN plot. The inset of Figure 4 shows a fit (solid line) of the experimental data (circles). The overall behavior of the FN plot exhibits an increase in the slope with the field value. The region, where the slope reduces, results from the imposed constraint of saturation of the CB current. The mode/trend with which the CB current acquires saturation is found to control the slope and shape of the intermediate region. The voltage value at which the CB saturates is deduced from Figure 2 (where the FN plot exhibits an onset of deviation from the linearity) and is taken to be 3.3 kV. It was possible to test various schemes of saturation so that a best fit of the numerical results with the experimental observations could be obtained. It is necessary to mention that the fit of the experimental curves is achieved after multiplying the total emission current by a fitting coefficient which arises from the fact that the collector

TABLE 1. Numerical Values of CB, VB, and Total Emission Currents of ZnO Semiconductor Calculated for β Factor of 2.1778×10^6 m^{-1}

voltage (*V*)	I_{CB} (A)	I_{VB} (A)	I_{total} (A)
3750	4.04×10^{-10}	1.99×10^{-12}	4.06×10^{-10}
4000	5.25×10^{-10}	2.65×10^{-11}	5.52×10^{-10}
4500	6.76×10^{-10}	9.33×10^{-10}	1.61×10^{-09}
5000	7.81×10^{-10}	1.63×10^{-08}	1.71×10^{-08}
5500	8.58×10^{-10}	1.70×10^{-07}	1.71×10^{-07}
6000	9.17×10^{-10}	1.21×10^{-06}	1.21×10^{-06}

current is a portion of the total emitted current due to the aperture effect of the probe−hole.

The comparison of FN plots of Figure 3 and Figure 4 emphasizes that only the assumption of CB current saturation is sufficient to justify the nonlinear behavior of the FN plot. The present model of calculation shows that the saturation value, imposed upon CB current, has no effect on the slope values in the low- and the high-fields regions. By changing the value of the saturation, the intermediate region of the FN plot shifts in position while the high- and the low-fields regions maintain their slope values. In addition, the assumption of the CB current saturation in the case of a semiconducting emitter is found to minimize the overestimation of the total emission current calculated for such an emitter according to the FN theory. This is because the total emission current is very sensitive to the contribution of the CB current, and any range/order of magnitude of the total current could be achieved by manipulating the CB current saturation. This justifies the differences in the ranges of Figures 3 and 4, because only due to the assumption of the CB saturation is a graph (Figure 4) in the same order of the emission current reproduced. It is difficult to estimate the aperture effect of the probe−hole due to the presence of other emitting pods. However, the fitting coefficient could provide us with an approximate value of the aperturing ratio, which was found to be ~7. The saturation value could be regarded as a key parameter in adjusting the total emission current. Table 1 shows an estimation of the contribution of the CB and the VB to the total emission current. The present analysis provides a strong justification for the comparable heights of the TED peaks (CB and VB peaks) reported earlier for the same specimens of the ZnO tetrapod structure.[17] Considering the experimental value of the β factor, the slope variation (slope ratio of the high-to-low fields regions) obtained from the present calculations is equal to 1.53, independent of the β value and correct within 8% with respect to the experimental ratio. However, the model calculation produces slightly higher values of the slopes in the low-field and the high-field regions. It is obviously true that the assumption of the CB current saturation may be justified with other certain effects (besides the limited generation rate of current carriers of Baskin *et al.*) and their influence on the final formulas, such as the

real internal distribution function and the density of occupied states which are different than that presently considered, despite being absent in the present analysis.

Regarding the contribution of the surface states to emission current and emission mechanism, Girard *et al.* (1997) studied the electronic structure of the (0001) surface of ZnO by angle-resolved photoelectron spectroscopy.[23] They recorded normal and off-normal emission spectra which gave valuable information about bulk and surface states, as well as the Zn 3d states. Two surface states were measured. One at 7.5 eV, which was predicted by theory and interpreted as arising from the backbonding of the Zn 4s−O2p mixed bulk states.[24,25] The other states are at 4.5 eV below Fermi level, which was not predicted theoretically but related to Zn 4p−O2p states. The Zn 3d states/electrons were either considered as core levels (some 7.5 eV below the VB maximum) or as part of the VB.[24,25] On the basis of these findings and the present analysis, the contribution of the surface states is not expected to be observed separately in the TEDs, though it will affect the FN plot behavior of the *I*−*V* characteristics. This may further justify the comparable heights of the two peaks in the TEDs, as emission from energy levels related to surface states may contribute to VB current.

CONCLUSIONS

Experimental probe−hole *I*−*V* characteristics of field emission from single tetrapods structures of ZnO have been reported. The nonlinearity of the FN plot and the mechanism of field emission have been explained by implementing a model calculation based on the saturation of the conduction band current and predominance of valence band current at high-field values. The model calculation is important for the fundamental understanding of the field emission mechanism in semiconducting ZnO. The simulated FN plots exhibit similar features to those observed experimentally. The model calculation suggests that the nonlinearity of the FN plot is a characteristic of the energy band structure and voltage-to-barrier-field conversion factor of the emitting material.

METHODS

ZnO tetrapod structures have been synthesized by the vapor deposition process, as described earlier.[8] A few structures were carefully mounted on a blunt tungsten (W) microtip with the help of vacuum compatible silver paste. The morphology of the tetrapod structures mounted on the blunt W tip was investigated using scanning electron microscope (SEM), JEOL6360A. The SEM images were recorded with an accelerating voltage of ~20 kV and filament current of ~60 μA. The probe−hole field emission studies were carried out in an all-metal chamber at a base pressure of 1×10^{-9} mbar. The mounting procedure of the specimen holder, the processing of ultrahigh vacuum in the experiment chamber, and the cleaning procedure of the specimen were mentioned earlier.[17] An indigenously fabricated probe−hole retarding field energy analyzer, similar to that described by Van Oostrom, was used for the measurements.[18] The design geometry of the analyzer provides us with the possibility of utilizing the probe−hole in obtaining the *I*−*V* characteristics by measuring the collector current *versus* the extracting voltage at constant operational conditions of lens to anode voltage ratio and constant emitter bias. The probe−hole is a 1 mm aperture made in the center of the anode of the analyzer to help measure the field emission characteristics from a very confined area of the emitter, and this setup assures the individuality of the electrons (i.e., emitted from a single pod) once measurements are taken from a single lobe of the emission pattern. A similar setup has been used in investigating field emission characteristics of carbon nanotubes whenever isolation of a single nanotube was practically difficult and a consistent interpretation of results was reported to be possible.[26]

Acknowledgment. A. A. Al-Tabbakh would like to acknowledge the financial support in the form of a Dr. D. S. Kothari Fellowship by UGC, India.

REFERENCES AND NOTES

1. Lee, C. J.; Lee, T. J.; Lyu, S. C.; Zhang, Y.; Ruh, H.; Lee, H. J. Field Emission from Well-Aligned Zinc Oxide Nanowires Grown at Low Temperature. *Appl. Phys. Lett.* **2002**, *81*, 3648–3650.
2. Wan, Q.; Yu, K.; Lin, C. L. Low-Field Electron Emission from Tetrapod-Like ZnO Nanostructures Synthesized by Rapid Evaporation. *Appl. Phys. Lett.* **2003**, *83*, 2253–2255.
3. Xu, C. X.; Sun, X. W. Field Emission From Zinc Oxide Nanopins. *Appl. Phys. Lett.* **2003**, *83*, 3806–3808.
4. Li, Y. B.; Bando, Y.; Golberg, D. ZnO Nanoneedles with Tip Surface Perturbations: Excellent Field Emitters. *Appl. Phys. Lett.* **2004**, *84*, 3603–3605.
5. Zhang, H.; Wang, R. M.; Zhu, Y. W. Effect of Adsorbates on Field-Electron Emission from ZnO Nanoneedle Arrays. *J. Appl. Phys.* **2004**, *96*, 624–628.
6. Shen, X.-P.; Yuan, A.-H.; Hu, Y.-M.; Jiang, Y.; Xu, Z.; Hu, Z. Fabrication, Characterization and Field Emission Properties of Large-Scale Uniform ZnO Nanotube Arrays. *Nanotechnology* **2005**, *16*, 2039–2043.
7. Ramgir, N. S.; Late, D. J; Bhise, A. B.; More, M. A.; Mulla, I. S.; Joag, D. S.; Pillai, V. K. ZnO Multipods, Submicron Wires and Spherical Structures and Their Unique Field Emission Behavior. *J. Phys. Chem. B* **2006**, *110*, 18236–18242.
8. Ramgir, N. S.; Mulla, I. S.; Pillai, V. K.; Late, D. J.; Bhise, A. B.; More, M. A.; Joag, D. S. Ultralow Threshold Field Emission from a Single Multipod Structure of ZnO. *Appl. Phys. Lett.* **2006**, *88*, 0421071−0421073.
9. Xing, Y. J.; Xi, Z. H.; Xue, Z. Q.; Zhang, X. D.; Song, J. H.; Wang, R. M.; Xu, J.; Song, Y.; Zhang, S. L.; Yu, D. P. Optical Properties of the ZnO Nanotubes Synthesized *via* Vapor Phase Growth. *Appl. Phys. Lett.* **2003**, *83*, 1689–1691.
10. Zhu, Z.; Chen, T.-L.; Gu, Y.; Warren, J.; Osgood, R. M. Zinc Oxide Nanowires Grown by Vapor-Phase Transport Using Selected Metal Catalysts: A Comparative Study. *J. Chem. Mater.* **2005**, *17*, 4227–4234.
11. Fowler, R. H.; Nordheim, L. Electron Emission in Intense Electric Fields. *Proc. R. Soc.* **1928**, *A119*, 173–185.
12. Murphy, E. L.; Good, R. H. Thermionic Emission, Field Emission and the Transition Region. *J. Phys. Rev.* **1956**, *102*, 1464–1473.
13. Stratton, R. Theory of Field Emission from Semiconductors. *Phys. Rev.* **1962**, *125*, 67–82.
14. Baskin, L. M.; Lvov, O. L.; Fursey, G. N. General Features of Field Emission from Semiconductors. *Phys. Stat. Sol. (b)* **1971**, *47*, 49–62.
15. Huang, Z. H.; Cutler, P. H.; Meskovesky, N. M.; Sullivan, T. E.

Calculation of Electron Field Emission from Diamond Surfaces. *J. Vac. Sci. Technol., B* **1994**, *13*, 526–530.
16. Rihon, N. Band Bending in Field Emission Spectroscopy from Zinc Oxide (0001) Polar Face. *Phys. Stat. Sol. (a)* **1981**, *63*, 617–625.
17. Al-Tabbakh, A. A.; More, M. A.; Joag, D. S.; Ramgir, N. S.; Mulla, I. S.; Pillai, V. K. Energy Analysis of Field Emitted Electrons from a ZnO Tetrapod. *Appl. Phys. Lett.* **2007**, *90*, 162102–162104.
18. Van Oostrom, A. G. J. *Validity of the Fowler−Nordheim Model for Field Electron Emission*; N. V. Philip:Eindhoven, The Netherlands, 1965; Vol. 49, pp 4−10.
19. Ling, X.; Guan-Qi, H.; Jian, W.; Hoi-Lam, T.; King-Fai, L.; Yu, Z.; Jun, X.; Xin-Fan, H.; Kok-Wai, C. Strong Electron Field Emission from Nano-CdS Modified Porous Silicon. *Chin. Phys. Lett.* **2004**, *21*, 2049–2054.
20. Joag, D. S. Adsorption and Diffusion Studies of Ni on Various Planes of W Using Field Emission Techniques. Ph.D. Thesis, University of Poona, Pune 411007, India, 1978.
21. Jaffe, J. E.; Snyder, J. A.; Lin, Z.; Hess, A. C. LDA and GGA Calculations for High-Pressure Phase Transitions in ZnO and MgO. *Phys. Rev. B* **2000**, *62*, 1660–1665.
22. Modinos, A. *Field, Thermionic and Secondary Electron Emission Spectroscopy*; 1984; Plenum Press: New York, pp 257−258.
23. Girard, R. T.; Tjernberg, O.; Chiaia, G.; Soderholm, S.; Karelsson, U. O.; Wigren, C.; Nylen, H.; Lindau, L. Electronic Structure of ZnO (0001) Studied by Angle-Resolved Photoelectron Spectroscopy. *Surf. Sci.* **1997**, *373*, 409–412.
24. Powell, R. A.; Spicer, W. E.; McMenamin, J. C. Location of the Zn 3d States in ZnO. *Phys. Rev. Lett.* **1971**, *27*, 97–99.
25. Powell, R. A.; Spicer, W. E.; McMenamin, J. C. Photoemission Studies of Wurtzite Zinc Oxide. *Phys. Rev. B* **1972**, *6*, 3056–3059.
26. Saito, Y.; Hamaguchi, K.; Hata, K.; Tohji, K.; Kasuya, A.; Nishina, Y.; Uchida, K.; Tasaka, Y.; Ikazaki, F.; Yumura, M. Field Emission from Carbon Nanotubes; Purified Single-Walled and Multi-Walled Tubes. *Ultramicroscopy* **1998**, *73*, 1–6.